European Radiology (2019) 29:6911–6921
https://doi.org/10.1007/s00330-019-06291-9

ONCOLOGY

Computed tomography textural analysis for the differentiation of chronic lymphocytic leukemia and diffuse large B cell lymphoma of Richter syndrome

C.P. Reinert[1] · B. Federmann[2] · J. Hofmann[1] · H. Bösmüller[2] · S. Wirths[3] · J. Fritz[4] · M. Horger[1]

Received: 14 March 2019 / Revised: 11 May 2019 / Accepted: 28 May 2019 / Published online: 24 June 2019

Abstract

Objective To test the hypothesis that both indolent and aggressive chronic lymphocytic leukemia (CLL) can be differentiated from diffuse large B cell lymphoma (DLBCL) of Richter syndrome (RS) by CT texture analysis (CTTA) of involved lymph nodes.

Material and methods We retrospectively included 52 patients with indolent CLL (26/52), aggressive CLL (8/52), and DLBCL of RS (18/52), who underwent standardized contrast-enhanced CT. In main lymphoma tissue, VOIs were generated from which CTTA features including first-, second-, and higher-order textural features were extracted. CTTA features were compared between the entire CLL group, the indolent CLL subtype, the aggressive CLL subtype, and DLBCL using a Kruskal-Wallis test. All p values were adjusted after the Bonferroni correction. ROC analyses for significant CTTA features were performed to determine cut-off values for differentiation between the groups.

Results Compared with DLBCL of RS, CTTA of the entire CLL group showed significant differences of entropy heterogeneity ($p < 0.001$), mean intensity ($p < 0.001$), mean average ($p = 0.02$), and number non-uniformity gray-level dependence matrix (NGLDM) ($p = 0.03$). Indolent CLL significantly differed for entropy ($p < 0.001$), uniformity of heterogeneity ($p = 0.02$), mean intensity ($p < 0.001$), and mean average ($p = 0.01$). Aggressive CLL showed significant differences in mean intensity ($p = 0.04$). For differentiation between CLL and DLBCL of RS, cut-off values for mean intensity and entropy of heterogeneity were defined (e.g., 6.63 for entropy heterogeneity [aggressive CLL vs. DLBCL]; sensitivity 0.78; specificity 0.63).

Conclusions CTTA features of ultrastructure and vascularization significantly differ in CLL compared with that in DLBCL of Richter syndrome, allowing complementary to visual features for noninvasive differentiation by contrast-enhanced CT.

Key Points

- *Richter transformation of CLL into DLBCL results in structural changes in lymph node architecture and vascularization that can be detected by CTTA.*
- *First-order CT textural features including intensity and heterogeneity significantly differ between both indolent CLL and aggressive CLL and DLBCL of Richter syndrome.*
- *CT texture analysis allows for noninvasive detection of Richter syndrome which is of prognostic value.*

H. Bösmüller and M. Horger contributed equally to this work.

Electronic supplementary material The online version of this article (https://doi.org/10.1007/s00330-019-06291-9) contains supplementary material, which is available to authorized users.

✉ C.P. Reinert
christian.reinert@med.uni-tuebingen.de

[1] Department of Diagnostic and Interventional Radiology, University Hospital Tübingen, Hoppe-Seyler-Str.3, 72076 Tübingen, Germany

[2] Department of Pathology and Neuropathology, University Hospital Tübingen, Liebermeisterstraße 8, 72076 Tübingen, Germany

[3] Department of Hematology and Oncology, University Hospital Tübingen, Otfried-Müller-Str. 10, 72076 Tübingen, Germany

[4] Russell H. Morgan Department of Radiology and Radiological, Johns Hopkins University School of Medicine, Science, 601 N. Caroline Street, JHOC 3142, Baltimore, MD 21287, USA

Keywords Texture analysis · Tomography, X-ray-computed · Leukemia, lymphocytic, chronic, B cell · Lymphoma, large B cell, diffuse

Abbreviations

CECT	Contrast-enhanced CT
CLL	Chronic lymphocytic leukemia
CTTA	CT texture analysis
DLBCL	Diffuse large B cell lymphoma
FDG	Fluorodeoxyglucose
LDH	Lactate dehydrogenase
ROI	Region of interest
RS	Richter syndrome
VOI	Volume of interest

Introduction

B cell chronic lymphocytic leukemia (CLL) is the most common chronic lymphoproliferative disease with a long and indolent course. The disease is characterized by proliferation of mature-appearing lymphocytes in the bone marrow, lymph nodes, and extra-lymphatic sites. Observation is often sufficient in the early stages, which present with no or subtle symptoms and have median survival times of greater than 10 years without therapy [1, 2]. However, advanced stages of CLL with enlarged lymph nodes and extramedullary involvement require systemic treatment.

During the course of the disease, CLL may take a more aggressive course with higher proliferation rates [3]. Up to 10% of CLL patients will undergo transformation into diffuse large B cell lymphoma, or less common Hodgkin's lymphoma, composite lymphoma, and interdigitating dendritic cell sarcoma (Richter syndrome) [4, 5].

The diagnosis of Richter syndrome is based on a combined assessment of clinical, laboratory, and imaging data. Rapidly enlarging lymph nodes, extra-lymphatic involvement of the liver, spleen and other tissue types, and bone marrow infiltration in conjunction with rapidly rising lactate dehydrogenase (LDH) level are suggestive for Richter syndrome [6]. In addition, positron emission tomography (PET) with abnormal ^{18}F-FDG (fluorodeoxyglucose) tracer accumulation of maximum standardized uptake value greater than five is considered highly suggestive for Richter syndrome [7]. However, standardized uptake values of advanced CLL with higher proliferation ratio can overlap with those of diffuse large B cell lymphoma (DLBCL), and even with other mimics of Richter syndrome, including viral and other lymph node infections [8–12]. In addition, chemotherapy and immunotherapies increase the likelihood of false-positive results, whereas newer biologic agents may inhibit glucose uptake and thus reduce standardized uptake values [13, 14].

The changing lymph node morphology that occurs during the transformation of CLL with lymphocyte-rich tissue into DLBCL with different amounts of vascularity and necrosis could represent an additional marker for the differentiation between the two entities [15]. Histologically, CLL consists of a diffuse architectural effacement due to a monotonous proliferation of small lymphocytes presenting with scant cytoplasm and a round nucleus with clumped chromatin, minimal mitotic activity, and a very low proliferation index [16, 17]. In contrast, large B lymphoid cells present with a nuclear size equal to or exceeding to that of macrophage nuclei or more than twice the size of a normal lymphocyte that is not present throughout the neoplasm [18–20]. Hence, macroscopically, a more heterogeneous attenuation of DLBCL is expected. While the clinical significance of the varying attenuation of different lymphoma types has been evaluated previously [21], computed tomography (CT) texture analysis is a novel histogram-based post-processing technique, which uses image data for ultrastructural tissue characterization and generation of quantitative imaging biomarkers that could be more accurate than qualitative assessments [22]. As tumor heterogeneity can be difficult to quantify with traditional imaging tools, CT texture analysis (CTTA) is a potentially useful biomarker that allows assessment and quantification of tumor spatial heterogeneity [23]. In various tumor types, e.g., colorectal cancer [24], esophageal cancer [25], lung cancer [26], head and neck cancer [27], and renal cell carcinoma [28], CTTA has shown promise in predicting pathologic features, response to therapy, and prognosis.

Therefore, the purpose of our study was to test the hypothesis that both indolent and aggressive CLL can be differentiated from DLBCL of Richter syndrome by CT texture analysis of involved lymph nodes.

Material and methods

Our study protocol was approved for retrospective evaluation of patient data by our institutional ethics committee with a waiver of the informed consent requirement (project number 467/2018).

We performed a retrospective search of our hospital information system for patients who underwent combined contrast-enhanced CT (CECT) and tissue sampling with sub-segment histopathological evaluation for Richter syndrome of CLL between March 2011 and May 2017. The search identified a total of 52 patients (19 female; mean age 70.3 ± 12.7 years), 26/52 (50%) patients with indolent CLL, 8/52 (15%) patients with aggressive CLL, and 18/52 (35%) patients with DLBCL

due to Richter syndrome. The patients with indolent CLL were classified according to the Binet classification into Binet A (12/26, 46%), Binet B (12/26, 46%), and Binet C (2/26, 8%) [29]. Aggressive CLL was defined clinically and radiologically by higher growth dynamics of involved lymph nodes and similarly classified as Binet A (2/8, 25%), Binet B (4, 50%), and Binet C (2/8, 25%).

Computed tomography protocol

CT was performed with patients in the supine position using 128-slice MDCT scanners (SOMATOM Definition AS+ or SOMATOM Definition Flash, Siemens Healthcare). Unenhanced and contrast-enhanced portal-venous phases were obtained using 120-kV photon energy, 200-mAs tube current, a soft tissue image reconstruction kernel, and 1-mm slice thickness for image reconstruction. A total of 100-mL iodine contrast agent (Iopromide, Ultravist 370, Bayer Vital) was given intravenously at a rate of 2 mL/s followed by a 30-mL saline chaser. Image acquisition began 65 s after the start of contrast agent injection. Image reconstruction was performed in all patients using filtered back projection.

Computed tomography texture analysis

CTTA data evaluation was performed using radiomics software (Siemens Healthcare) that is based on the pyradiomics package, a python package for the extraction of radiomics features from medical imaging [30]. CTTA was applied on image data sets that were reconstructed with 1-mm slice thickness. In patients with aggressive CLL and patients with DLBCL of RS, only enlarged lymph nodes which were biopsied or excised for histopathological proofing after imaging were selected for CTTA. In patients with indolent CLL, representative (enlarged) lymph nodes in the axilla, mediastinum, or retroperitoneum were selected for measurement. There was no extranodal Richter syndrome (RS) in our cohort. The regions of interests (ROIs) were drawn manually in lymph nodes under exclusion of neighboring tissues like blood vessels and visibly necrotic areas. This procedure of ROI setting was performed by two radiologists in consensus with an experience of 2 years and 5 years in CTTA. To provide comparability for all data sets, standardized measurements were performed. All set ROIs were used to generate the specific volume of interests (VOIs). The computation of each texture type for an input volume of interest involved assigning a new value ("texture value") to all voxels of that volume of interest and thus creating a "texture image." The first step consisted of image filtration for selectively extracting features of different sizes and intensity variation. The image filtration-histogram technique extracts texture features of different sizes followed by histogram quantification as described by Miles et al [31]. In the second step, quantification of tissue texture was performed using series of derived images displaying features at different spatial scales from fine (2 mm in radius) to coarse texture (6 mm in radius) within a volume of interest (Fig. 1). Window ranges of 0 to 400 HU were used. Computation was performed on the current voxel and its neighborhood, and the results of that were stored as the texture value of the current voxel. This was repeated for every voxel in the volume of interest. The texture type defined the specific kind of computation that was performed, including heterogeneity, intensity, deviation, average, skewness, entropy of co-occurrence, number non-uniformity gray-level dependence matrix (NGLDM), entropy NGLDM, and contrast neighboring gray tone difference matrix (NGTDM). For all these parameters, the mean, entropy, and uniformity were calculated.

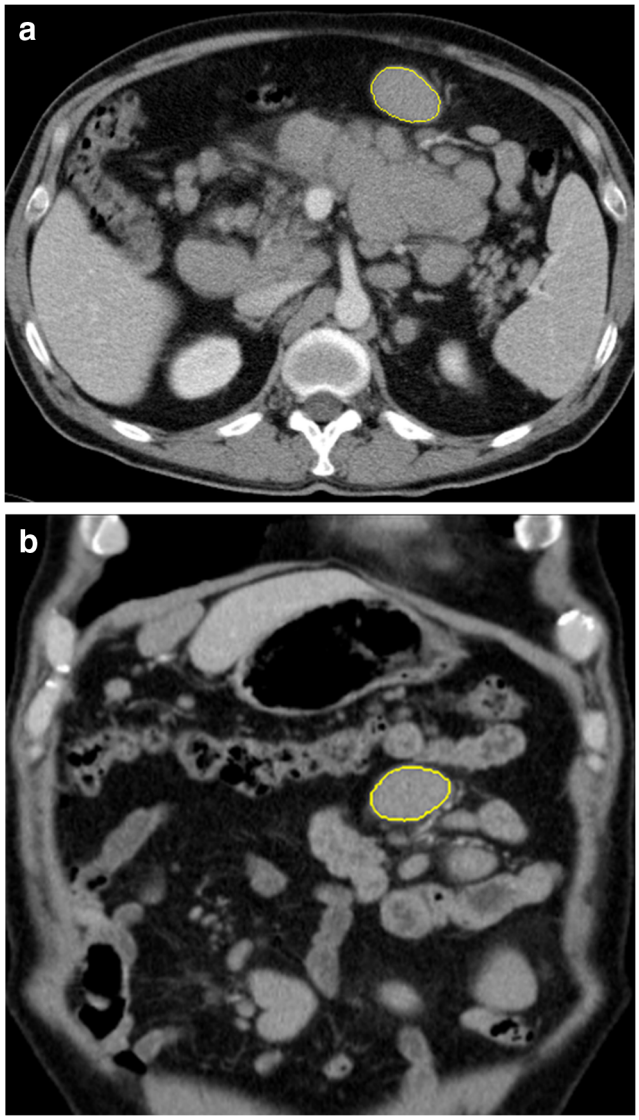

Fig. 1 A 56-year-old male patient with DLBCL of Richter syndrome and involved mesenteric lymph nodes. Axial (**a**) and coronal (**b**) CT images showing a lymphoma mass in which a volume of interest was drawn for CT texture analysis, thereby excluding other anatomical structures, such as adjacent vessels

The definition of each of these parameters is given as supplemental material (Table 4). For the final evaluation, we used the coarse filter. We first compared the group of CLL with DLBCL, and then both the indolent and aggressive CLL subtypes separately against DLBCL.

Histology

Histological criteria for the diagnosis of DLBCL were a diffuse effacement of lymph nodes or extranodal sites with sheets of large cells with centroblastic, immunoblastic, or anaplastic morphology and a starry-sky pattern with apoptosis and tumor necrosis [18]. In contrast, the histological criteria for CLL were an infiltrate consisting of small round lymphocytes with dense chromatin, sparse cytoplasm, and low mitotic activity [32].

Statistical analysis

Statistical analysis was performed using SPSS Version 22 (IBM Corporation). All parameters were tested by the Kolmogorov-Smirnov test for the normality. The Kruskal-Wallis test was used to compare textural features between the entire CLL group, indolent CLL, aggressive CLL, and DLBCL of Richter syndrome. To address the multiple comparisons, a Bonferroni correction was applied. The adjusted p values were considered significant at a level of 0.05. The predictive performance was assessed by estimating predictive values (positive predictive value [PPV] and negative predictive value [NPV]), sensitivity and specificity, and the area under the curve (AUC) with receiver operating characteristic (ROC) curves. The ROC curve was generated by computing sensitivity and specificity at each observed cut-off. The optimal cut-off values are derived from the point on the ROC curve with the minimum distance to the upper-left corner (where sensitivity and specificity equal 1, respectively).

Results

Computed tomography texture analysis of indolent CLL and DLBCL of Richter syndrome

CTTA values between patients with indolent CLL and patients with DLBCL of Richter syndrome demonstrated significant differences of mean intensity (indolent CLL, 66.68 ± 10.99; DLBCL, 54.18 ± 14.83; $p < 0.001$), entropy of heterogeneity (indolent CLL, 2.96 ± 3.46; DLBCL, 6.36 ± 2.34; $p < 0.001$) (Fig. 2), uniformity of heterogeneity (indolent CLL, 0.005 ± 0.004; DLBCL, 0.008 ± 0.004; $p = 0.02$), and mean average (indolent CLL, 67.89 ± 16.35; DLBCL, 53.89 ± 14.83; $p = 0.01$) (Table 1). For the differentiation between indolent CLL and DLBCL of Richter syndrome, receiver operating characteristic analysis derived 6.68 as the cut-off value for entropy of heterogeneity (sensitivity 0.78, specificity 0.73, PPV 0.67, NPV 0.83) and 58.56 as the cut-off value for mean intensity (sensitivity 0.81, specificity 0.72, PPV 0.67, NPV 0.84) (Fig. 3).

Computed tomography texture analysis of aggressive CLL and DLBCL of Richter syndrome

CTTA values between patients with aggressive CLL and patients with DLBCL of Richter syndrome demonstrated

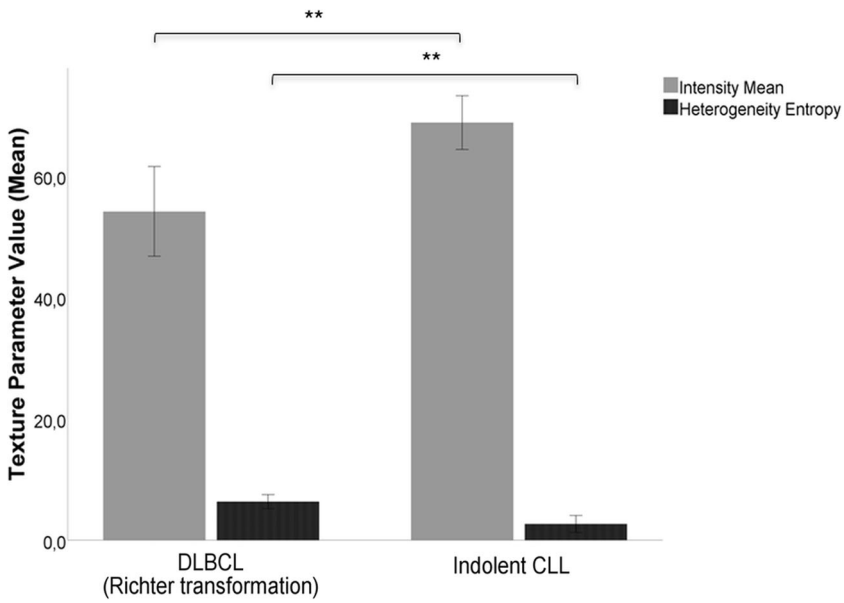

Fig. 2 Texture parameter values of intensity mean and heterogeneity entropy in patients with DLBCL (Richter transformation, $n = 18$) compared with that in the indolent group of CLL patients ($n = 26$). A Kruskal-Wallis test was applied. Adjusted p values are shown after Bonferroni correction. ** = $p < 0.001$

Table 1 Computed tomography texture analysis values in patients with indolent CLL (n = 26) and patients with DLBCL of Richter syndrome (n = 18) on portal-venous phase CT images using a coarse filter. A Kruskal-Wallis test was applied. P values have been adjusted after Bonferroni correction. ** $p < 0.001$; * $p < 0.05$

	CLL (indolent course)			DLBCL (Richter syndrome)			p value (CLL vs. DLBCL)		
Coarse Filter	Mean	Entropy	Uniformity	Mean	Entropy	Uniformity	Mean	Entropy	Uniformity
Heterogeneiy	-0.04	2.96	0.005	-0.02	6.36	0.008	.75	< .001**	.02*
Intensity	66.68	5.79	0.02	54.18	5.78	0.02	< .001**	1.0	1.0
Average	67.89	3.64	0.13	53.89	3.99	0.09	.01*	.28	.24
Deviation	22.82	3.27	0.17	17.71	3.28	0.16	.27	1.0	1.0
Skewness	-0.04	3.89	0.24	-0.002	4.87	0.11	1.0	.10	.23
Entropy (Co-occurence Matrix)	0.55	5.76	0.11	0.34	5.74	0.18	.33	.77	1.0
Difference Variance (Co-occurence Matrix)	0.09	5.19	0.12	0.05	4.91	0.19	.20	1.0	1.0
Number non-uniformity (NGLDM)	0.62	4.15	0.22	0.76	4.04	0.24	.07	1.0	.68
Entropy (NGLDM)	1.14	6.07	0.09	1.10	6.76	0.02	.54	.25	.50
Contrast (NGTDM)	116.98	3.48	0.43	89.82	3.40	0.43	1.0	.91	1.0

significant differences of mean intensity (aggressive CLL, 64.65 ± 6.61; DLBCL, 54.18 ± 14.83; $p = 0.04$) using a coarse filter (Fig. 4). The entropy of heterogeneity was higher in DLBCL of RS (6.36 ± 2.34) than in aggressive CLL (5.02 ± 3.12) without statistical significance ($p = 0.06$) (Fig. 4; Table 2). For the differentiation between aggressive CLL and DLBCL of Richter syndrome, receiver operating characteristic analysis derived 6.63 as the cut-off value for the entropy of heterogeneity (sensitivity 0.78, specificity 0.63, PPV 0.82, NPV 0.56) and 58.63 as the cut-off value for mean intensity (sensitivity 0.75, specificity 0.72, PPV 0.86, NPV 0.56) (Fig. 5).

Computed tomography texture analysis of combined indolent and aggressive CLL and DLBCL of Richter syndrome

CTTA values between the groups including patients with indolent and aggressive CLL and patients with DLBCL of Richter syndrome demonstrated significant differences of

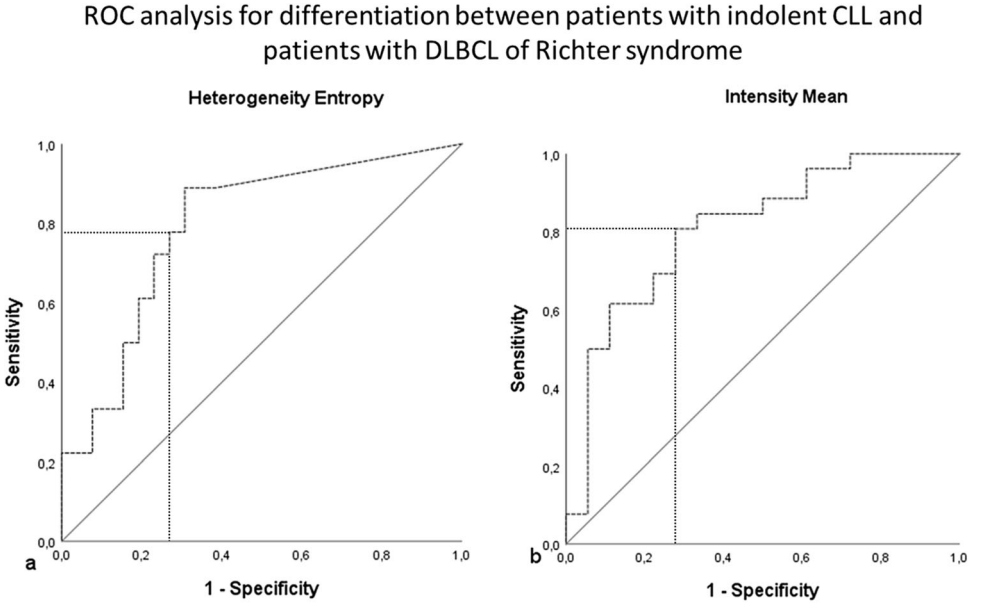

	Filter	AUC	95% CI	Cut-off-value	Sensitivity	Specificity	P
Heterogeneity Entropy	Coarse	0.79	0.66 – 0.93	6.68	0.78	0.73	< .001
Intensity Mean	Coarse	0.81	0.67 – 0.94	58.56	0.81	0.72	< .001

Fig. 3 Receiver operating characteristic (ROC) analysis based on the texture parameters heterogeneity entropy (**a**) and intensity mean (**b**) which have been proven to be significantly different between patients with indolent CLL and patients with DLBCL of Richter syndrome. Discriminating cut-off values have been determined for optimal differentiation between the two groups

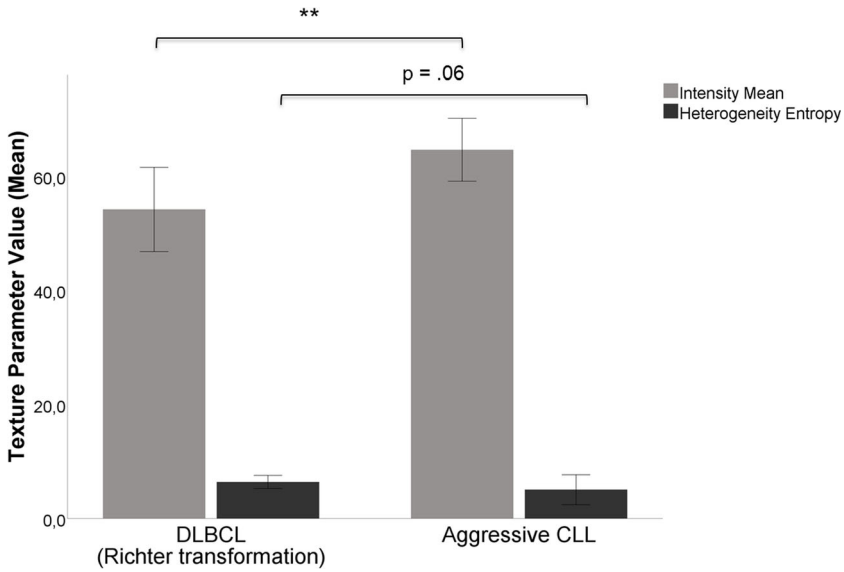

Fig. 4 Texture parameter values of intensity mean and heterogeneity entropy in patients with DLBCL (Richter transformation, $n = 18$) compared with that in the aggressive group of CLL patients ($n = 8$). A Kruskal-Wallis test was applied. Adjusted p values are shown after Bonferroni correction. ** = $p < 0.001$

mean intensity (CLL, 67.85 ± 10.20; DLBCL, 54.18 ± 14.83; $p < 0.001$), entropy of heterogeneity (CLL, 3.22 ± 3.49; DLBCL, 6.36 ± 2.34; $p < 0.001$), mean average (CLL, 66.23 ± 14.98; DLBCL, 53.89 ± 14.83; $p = 0.02$), and number non-uniformity gray-level dependence matrix (NGLDM) (CLL, 0.61 ± 0.23; DLBCL, 0.76 ± 0.35; $p = 0.03$) using a coarse filter (Fig. 6; Table 3). For the differentiation between all CLL and DLBCL of Richter syndrome, receiver operating characteristic analysis derived for 6.86 as the cut-off value for the entropy of heterogeneity (sensitivity 0.81, specificity 0.74, PPV 0.63, NPV 0.88) and 58.56 as the cut-off value for mean intensity (sensitivity 0.79, specificity 0.72, PPV 0.60, NPV 0.86) (Fig. 7).

Discussion

We performed a standardized CT texture analysis of contrast-enhanced CT image data in order to quantify ultrastructural tissue differences and differences in the intensity and distribution of contrast enhancement between two lymphoma types. Our results show significant differences in first-order CT textural features, which may allow for CT-based differentiation and diagnosis of CLL transformation into DLBCL.

In this study, we first compared CTTA features of indolent CLL with those of DLBCL of RS and found significant differences in terms of mean intensity and average (noise-corrected image intensity) which proved higher in CLL,

Table 2 Computed tomography texture analysis values in patients with aggressive CLL ($n = 8$) and patients with DLBCL of Richter syndrome ($n = 18$) on portal-venous phase CT images using a coarse filter. A Kruskal-Wallis test was applied. P values have been adjusted after Bonferroni correction. * $p < 0.05$

	CLL (aggressive course)			DLBCL (Richter syndrome)			p value (CLL vs. DLBCL)		
Coarse Filter	Mean	Entropy	Uniformity	Mean	Entropy	Uniformity	Mean	Entropy	Uniformity
Heterogeneiy	-0.0004	5.02	0.01	-0.02	6.36	0.01	.92	.06	.73
Intensity	64.65	5.82	0.02	54.18	5.78	0.02	.04*	1.0	1.0
Average	62.75	3.71	0.09	53.89	3.99	0.09	.29	.73	.62
Deviation	17.31	2.85	0.19	17.71	3.28	0.16	1.0	.73	.62
Skewness	-0.0004	4.53	0.13	-0.002	4.87	0.11	.48	1.0	.99
Entropy (Co-occurence Matrix)	0.71	6.42	0.05	0.34	5.74	0.18	.16	1.0	1.0
Difference Variance (Co-occurence Matrix)	0.10	5.40	0.06	0.05	4.91	0.19	.20	1.0	1.0
Number non-uniformity (NGLDM)	0.66	4.69	0.17	0.76	4.04	0.24	.52	.92	.35
Entropy (NGLDM)	1.19	6.65	0.02	1.10	6.76	0.02	1.0	1.0	.1.0
Contrast (NGTDM)	171.62	4.51	0.32	89.82	3.40	0.43	.73	.68	.57

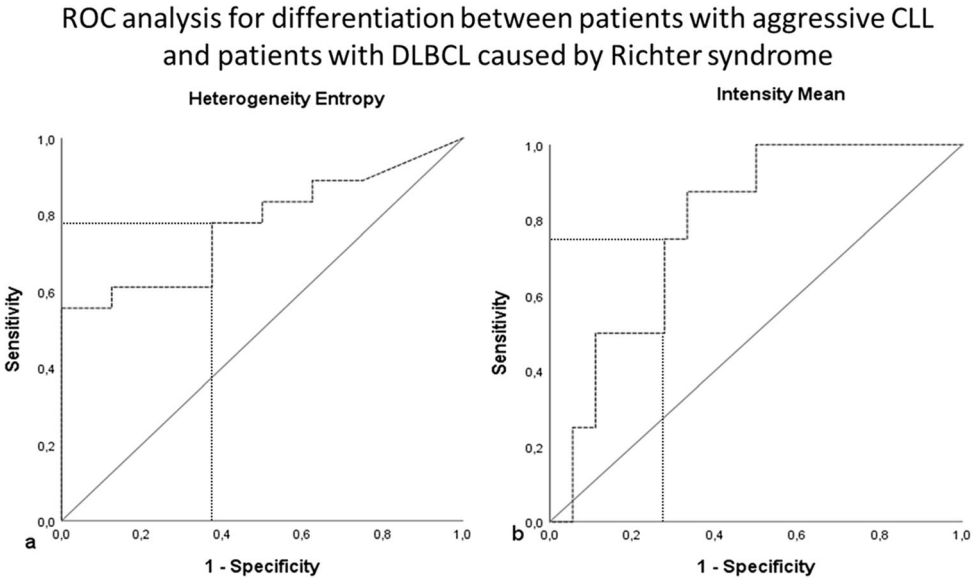

Fig. 5 Receiver operating characteristic (ROC) analysis based on the texture parameters heterogeneity entropy (**a**) and intensity mean (**b**). Intensity mean has been proven to be significantly different between patients with aggressive CLL and patients with DLBCL of Richter syndrome. Discriminating cut-off values have been determined for optimal differentiation between the two groups

	Filter	AUC	95% CI	Cut-off-value	Sensitivity	Specificity	P
Heterogeneity Entropy	Coarse	0.77	0.59 – 0.95	6.63	0.78	0.63	0.06
Intensity Mean	Coarse	0.79	0.61 – 0.96	58.63	0.75	0.72	0.04

entropy of heterogeneity which was double as high for DLBCL of RS, and uniformity of heterogeneity which was lower in DLBCL of RS. These CTTA features are reflecting higher tissue attenuation in CLL (mean intensity) and higher tissue heterogeneity of DLBCL of RS (higher entropy and lower uniformity of heterogeneity). As we applied CTTA on contrast-enhanced CT image data, the calculated textural features are expected to reflect both ultrastructural tissue properties as well as differences in the vascular network between the investigated lymphoma types. The lower mean intensity (attenuation) values of DLBCL of RS were therefore surprising as the microvascular density of CLL should be similar when compared with that of DLBCL, or even increased in DLBCL [33, 34]. However, microvascular areas of the DLBCL are known to show more variability, and interspaced areas of tumor necrosis and apoptosis are

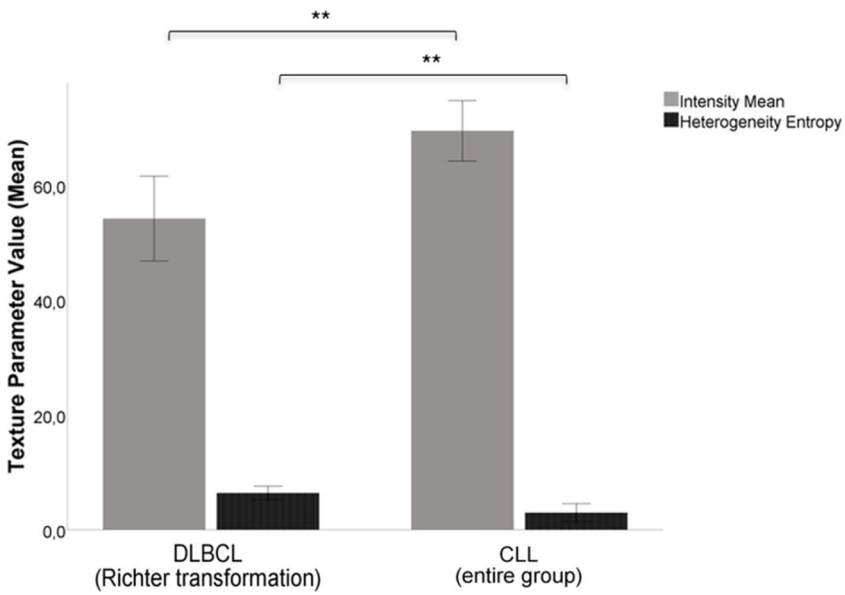

Fig. 6 Texture parameter values of intensity mean and heterogeneity entropy in patients with DLBCL (Richter transformation, $n = 18$) compared with that in the entire group of CLL patients (both the indolent and aggressive subtype, $n = 34$). A Kruskal-Wallis test was applied. Adjusted p values are shown after Bonferroni correction. ** = $p < 0.001$

Table 3 Computed tomography texture analysis values in patients with indolent and aggressive CLL (n = 34) and patients with DLBCL of Richter syndrome (n = 18) on portal-venous phase CT images using a coarse filter. A Kruskal-Wallis test was applied. p values have been adjusted after Bonferroni correction. ** $p < 0.001$; $p < 0.05$

	CLL (indolent and aggressive course)			DLBCL (Richter syndrome)			p value (CLL vs. DLBCL)		
Coarse Filter	Mean	Entropy	Uniformity	Mean	Entropy	Uniformity	Mean	Entropy	Uniformity
Heterogeneiy	-0.02	3.22	0.01	-0.02	6.36	0.008	.49	< .001**	.22
Intensity	67.85	5.77	0.02	54.18	5.78	0.02	< .001**	.99	.92
Average	66.23	3.68	0.11	53.89	3.99	0.09	.02*	.40	.40
Deviation	21.98	3.18	0.17	17.71	3.28	0.16	.43	1.0	1.0
Skewness	-0.02	4.01	0.21	-0.002	4.87	0.11	1.0	.51	.95
Entropy (Co-occurence Matrix)	0.59	6.02	0.08	0.34	5.74	0.18	.06	1.0	1.0
Difference Variance (Co-occurence Matrix)	0.09	5.35	0.09	0.05	4.91	0.19	.08	1.0	.95
Number non-uniformity (NGLDM)	0.61	4.47	0.18	0.76	4.04	0.24	.03*	.76	.11
Entropy (NGLDM)	1.25	6.27	0.07	1.10	6.76	0.02	.37	.79	1.0
Contrast (NGTDM)	126.77	3.501	0.44	89.82	3.40	0.43	1.0	1.0	1.0

presumed to be responsible for a lower mean attenuation on CECT irrespective of the visual presence of larger areas of necrosis [35]. Based on our results, one may speculate that the vessel wall permeability and thus diffusion of contrast medium in the extravascular space are greater in CLL; however, we were unable to further assess this finding as no tumor perfusion data were available in our cohort. Nevertheless, these results indicate the existence of sufficiently accurate cut-off values that may allow the differentiation of indolent CLL from DLBCL of Richter syndrome, including 58.56 for mean intensity and 6.68 for entropy heterogeneity. Second, we separately evaluated the subgroup of aggressive CLL which is expected to show more similarities with the aggressive DLBCL of RS and, indeed, we found only one significant difference between the two which was again the mean intensity. The calculated cut-off values of 58.63 for mean intensity

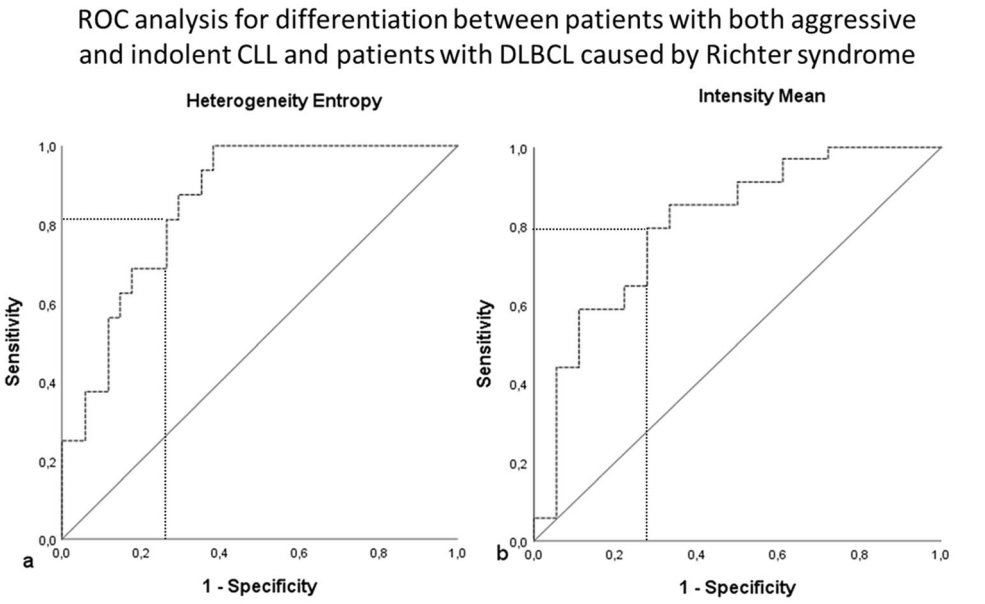

	Filter	AUC	95% CI	Cut-off-value	Sensitivity	Specificity	P
Heterogeneity Entropy	Coarse	0.85	0.75 – 0.96	6.86	0.81	0.74	< .001
Intensity Mean	Coarse	0.80	0.67 – 0.93	58.56	0.79	0.72	< .001

Fig. 7 Receiver operating characteristic (ROC) analysis based on the texture parameters heterogeneity entropy (**a**) and intensity mean (**b**) which have been proven to be significantly different between patients with both indolent and aggressive CLL and patients with DLBCL of Richter syndrome. Discriminating cut-off values have been determined for optimal differentiation between the two groups

and 6.63 for entropy heterogeneity (which also differed but not reaching statistical significance) may therefore also allow the differentiation of aggressive CLL from DLBCL of RS. Finally, similar cut-off values apply to the entire group of CLL for differentiation from DLBCL of RS. Comparing all CLL patients with DLBCL of RS patients yielded additionally a significant difference in NGLDM. The separate assessment of the two subgroups of CLL with lower extramedullary tumor burden / low growth dynamic and CLL with rapidly enlarging lymph nodes and hepatosplenomegaly but no histopathology evidence of Richter transformation showed similarly significant differences to DLBCL with lower values of mean intensity and mean average as well as higher values of entropy of heterogeneity for DLBCL. Notably, mean intensity and entropy of heterogeneity values were significantly different in the more aggressive CLL group than in DLBCL of RS. Pathology findings in all patients were consulted for understanding our CTTA results.

The need for additional imaging markers was our motivation for the evaluation of CT texture analysis for the differentiation of CLL and DLBCL of Richter syndrome. The Richter transformation occurs generally at a single location. CT morphologic changes at follow-up may suggest this complication, but the complementary characterization of such findings, e.g., by means of CTTA, would be wishful and we therefore believe that this post-processing tool could enhance the diagnostic accuracy of CT in this respect.

The role of first-order textural features and, in particular, of tumor heterogeneity for tumor assessment as well as its implications for prognosis and for treatment response monitoring has been evaluated previously in other tumor entities [36–38]. Lubner et al found that pretreatment tumor heterogeneity in primary renal cell carcinomas correlates with histology and clinical outcome [22]. Ganeshan et al found strong correlations between the esophageal tumor heterogeneity, tumor metabolism, stage, and survival [25]. The same authors found similar results in non-small cell lung carcinomas where tumor heterogeneity predicted survival [26]. In a report by Ng et al, tumor heterogeneity predicted 5-year survival in colorectal carcinomas [24]. Many other studies focused on the overall benefit of using CTTA features for tumor characterization, discrimination, for prediction of response to therapy, and survival [39–41]. Goh et al reported a continuous decrease in the heterogeneity of renal cell carcinomas during successful treatment with tyrosine kinase inhibitors [42].

Our study has limitations. First, image data evaluation was performed retrospectively and the number of patients is limited. This could have impacted the examination protocol and the CTTA quantification results. However, at our institution, CT protocols including the administered contrast agent volume are standardized which minimizes variability of used imaging parameters. Nevertheless, the contrast agent volume was not adapted to body weight and, therefore, this might have influenced to some extent the quantification of tissue attenuation and related CTTA features (e.g., mean intensity). Second, we did not address extranodal involvement by Richter transformation in order to ensure comparability of results. Third, we used only a limited number of CT textural features in order to limit the complexity of the results. However, the most frequently applied and robust textural features are those of the first-order and in particular the heterogeneity which has been by far most often used as a noninvasive surrogate for spatial heterogeneity in cellular density, angiogenesis (if contrast-enhanced studies are evaluated as in our own study), and necrosis. Moreover, these features are less affected by image noise.

In conclusion, CTTA features of ultrastructure and vascularization are significantly different in patients with CLL compared with those with DLBCL of Richter syndrome, which may allow complementary to visual features for a noninvasive differentiation by contrast-enhanced CT.

Funding The authors state that this work has not received any funding.

Compliance with ethical standards

Guarantor The scientific guarantor of this publication is Dr. Christian Philipp Reinert.

Conflict of interest Marius Horger received institutional research funds and speaker's honorarium from Siemens Healthineers and is a scientific advisor of Siemens Healthcare, Germany. Konstantin Nikolaou received institutional research funds and speaker's honorarium from Siemens Healthineers and is a scientific advisor of Siemens Healthcare, Germany. Jan Fritz received institutional research support from Siemens Healthcare, USA, DePuy, Zimmer, Microsoft, and BTG International; is a scientific advisor of Siemens Healthcare USA, Alexion Pharmaceuticals, and BTG International; received speaker's honorarium from Siemens Healthcare, USA; and has shared patents with Siemens Healthcare and Johns Hopkins University. The other authors have declared that no competing interests exist.

Statistics and biometry Dr. Christian Philipp Reinert has significant statistical expertise.

Informed consent Written informed consent was waived by the Institutional Review Board (project number 467/2018).

Ethical approval Institutional Review Board approval was obtained.

Methodology
- retrospective
- diagnostic study
- performed at one institution

References

1. Lynch RC, Gratzinger D, Advani RH (2017) Clinical impact of the 2016 update to the WHO lymphoma classification. Curr Treat Options Oncol 18(45)

2. (1990) Effects of chlorambucil and therapeutic decision in initial forms of chronic lymphocytic leukemia (stage A): results of a randomized clinical trial on 612 patients. The French Cooperative Group on Chronic Lymphocytic Leukemia. Blood 75:1414–1421
3. Hallek M (2017) Chronic lymphocytic leukemia: 2017 update on diagnosis, risk stratification, and treatment. Am J Hematol 92:946–965
4. Tsimberidou AM, O'Brien S, Kantarjian HM et al (2006) Hodgkin transformation of chronic lymphocytic leukemia: the M. D. Anderson Cancer Center experience. Cancer 107:1294–1302
5. Vitale C, Ferrajoli A (2016) Richter syndrome in chronic lymphocytic leukemia. Curr Hematol Malig Rep 11:43–51
6. Jain P, O'Brien S (2012) Richter's transformation in chronic lymphocytic leukemia. Oncology (Williston Park) 26:1146–1152
7. Niemann CU, Polliack A, Hutchings M (2014) Suspected Richter transformation: positron emission tomography/computed tomography tells us who should have a biopsy and where. Leuk Lymphoma 55:233–234
8. Grozinger G, Adam P, Horger M (2014) HSV lymphadenitis in chronic lymphocytic leukemia – a rare but difficult differential diagnosis. Rofo 186:79–80
9. Liu Y (2011) Demonstrations of AIDS-associated malignancies and infections at FDG PET-CT. Ann Nucl Med 25:536–546
10. Mhlanga JC, Durand D, Tsai HL et al (2014) Differentiation of HIV-associated lymphoma from HIV-associated reactive adenopathy using quantitative FDG PET and symmetry. Eur J Nucl Med Mol Imaging 41:596–604
11. Bruzzi JF, Macapinlac H, Tsimberidou AM et al (2006) Detection of Richter's transformation of chronic lymphocytic leukemia by PET/CT. J Nucl Med 47:1267–1273
12. Papajík T, Mysliveček M, Urbanová R et al (2014) 2-[18F]fluoro-2-deoxy-D-glucose positron emission tomography/computed tomography examination in patients with chronic lymphocytic leukemia may reveal Richter transformation. Leuk Lymphoma 55:314–319
13. Ansell SM, Armitage JO (2012) Positron emission tomographic scans in lymphoma: convention and controversy. Mayo Clin Proc 87:571–580
14. Dubreuil J, Salles G, Bozzetto J et al (2017) Usual and unusual pitfalls of 18F-FDG-PET/CT in lymphoma after treatment: a pictorial review. Nucl Med Commun 38:563–576
15. Song MK, Chung JS, Shin DY et al (2017) Tumor necrosis could reflect advanced disease status in patients with diffuse large B cell lymphoma treated with R-CHOP therapy. Ann Hematol 96:17–23
16. Soilleux EJ, Wotherspoon A, Eyre TA, Clifford R, Cabes M, Schuh AH (2016) Diagnostic dilemmas of high-grade transformation (Richter's syndrome) of chronic lymphocytic leukaemia: results of the phase II National Cancer Research Institute CHOP-OR clinical trial specialist haemato-pathology central review. Histopathology 69:1066–1076
17. Swerdlow SH, Campo E, Harris NL et al (2017) WHO classification of tumours of haematopoietic and lymphoid tissues. International Agency for Research on Cancer
18. Rossi D, Spina V, Deambrogi C et al (2011) The genetics of Richter syndrome reveals disease heterogeneity and predicts survival after transformation. Blood 117:3391–3401
19. Pathania K (2009) Richter's syndrome. Med J Armed Forces India 65:375–377
20. Saito A, Takashima S, Takayama F, Kawakami S, Momose M, Matsushita T (2001) Spontaneous extensive necrosis in non-Hodgkin lymphoma: prevalence and clinical significance. J Comput Assist Tomogr 25:482–486
21. Adams HJA, de Klerk JMH, Fijnheer R et al (2016) Tumor necrosis at FDG-PET is an independent predictor of outcome in diffuse large B-cell lymphoma. Eur J Radiol 85:304–309
22. Lubner MG, Smith AD, Sandrasegaran K, Sahani DV, Pickhardt PJ (2017) CT texture analysis: definitions, applications, biologic correlates, and challenges. Radiographics 37:1483–1503
23. Ganeshan B, Miles KA (2013) Quantifying tumour heterogeneity with CT. Cancer Imaging 13:140–149
24. Ng F, Ganeshan B, Kozarski R, Miles KA, Goh V (2013) Assessment of primary colorectal cancer heterogeneity by using whole-tumor texture analysis: contrast-enhanced CT texture as a biomarker of 5-year survival. Radiology 266:177–184
25. Ganeshan B, Skogen K, Pressney I, Coutroubis D, Miles K (2012) Tumour heterogeneity in oesophageal cancer assessed by CT texture analysis: preliminary evidence of an association with tumour metabolism, stage, and survival. Clin Radiol 67:157–164
26. Ganeshan B, Panayiotou E, Burnand K, Dizdarevic S, Miles K (2012) Tumour heterogeneity in non-small cell lung carcinoma assessed by CT texture analysis: a potential marker of survival. Eur Radiol 22:796–802
27. Zhang H, Graham CM, Elci O et al (2013) Locally advanced squamous cell carcinoma of the head and neck: CT texture and histogram analysis allow independent prediction of overall survival in patients treated with induction chemotherapy. Radiology 269:801–809
28. Leng S, Takahashi N, Gomez Cardona D et al (2017) Subjective and objective heterogeneity scores for differentiating small renal masses using contrast-enhanced CT. Abdom Radiol (NY) 42:1485–1492
29. Binet JL, Auquier A, Dighiero G et al (1981) A new prognostic classification of chronic lymphocytic leukemia derived from a multivariate survival analysis. Cancer 48:198–206
30. van Griethuysen JJM, Fedorov A, Parmar C et al (2017) Computational radiomics system to decode the radiographic phenotype. Cancer Res 77:e104–e107
31. Miles KA, Ganeshan B, Hayball MP (2013) CT texture analysis using the filtration-histogram method: what do the measurements mean? Cancer Imaging 13:400–406
32. Mao Z, Quintanilla-Martinez L, Raffeld M et al (2007) IgVH mutational status and clonality analysis of Richter's transformation: diffuse large B-cell lymphoma and Hodgkin lymphoma in association with B-cell chronic lymphocytic leukemia (B-CLL) represent 2 different pathways of disease evolution. Am J Surg Pathol 31:1605–1614
33. Spira D, Adam P, Linder C et al (2012) Perfusion and flow extraction product as potential discriminators in untreated follicular and diffuse large B cell lymphomas using volume perfusion CT with attempt at histopathologic explanation. AJR Am J Roentgenol 198:1239–1246
34. Ruan J, Hajjar K, Rafii S, Leonard JP (2009) Angiogenesis and antiangiogenic therapy in non-Hodgkin's lymphoma. Ann Oncol 20:413–424
35. Cardesa-Salzmann TM, Colomo L, Gutierrez G et al (2011) High microvessel density determines a poor outcome in patients with diffuse large B-cell lymphoma treated with rituximab plus chemotherapy. Haematologica 96:996–1001
36. Yip C, Davnall F, Kozarski R et al (2015) Assessment of changes in tumor heterogeneity following neoadjuvant chemotherapy in primary esophageal cancer. Dis Esophagus 28:172–179
37. Ganeshan B, Miles KA, Babikir S et al (2017) CT-based texture analysis potentially provides prognostic information complementary to interim fdg-pet for patients with hodgkin's and aggressive non-hodgkin's lymphomas. Eur Radiol 27:1012–1020
38. Durot C, Mulé S, Soyer P, Marchal A, Grange F, Hoeffel C (2019) Metastatic melanoma: pretreatment contrast-enhanced CT texture parameters as predictive biomarkers of survival in patients treated with pembrolizumab. Eur Radiol 29:3183–3191. https://doi.org/10.1007/s00330-018-5933-x

39. Feng C, Lu F, Shen Y et al (2018) Tumor heterogeneity in gastrointestinal stromal tumors of the small bowel: volumetric CT texture analysis as a potential biomarker for risk stratification. Cancer Imaging 18:46
40. Starkov P, Aguilera TA, Golden DI et al (2019) The use of texture-based radiomics CT analysis to predict outcomes in early-stage non-small cell lung cancer treated with stereotactic ablative radiotherapy. Br J Radiol 92:20180228
41. Lee SJ, Zea R, Kim DH, Lubner MG, Deming DA, Pickhardt PJ (2018) CT texture features of liver parenchyma for predicting development of metastatic disease and overall survival in patients with colorectal cancer. Eur Radiol 28:1520–1528
42. Goh V, Ganeshan B, Nathan P, Juttla JK, Vinayan A, Miles KA (2011) Assessment of response to tyrosine kinase inhibitors in metastatic renal cell cancer: CT texture as a predictive biomarker. Radiology 261:165–171